International Communications in Heat and Mass Transfer

https://www.journals.elsevier.com/international-communications-in-heat-and-mass-transfer

Impact factor = 6.782

Accepted September 3rd 2022

Dynamics of tangent-hyperbolic nanoliquids configured by stratified extending surface: Effects of transpiration, Robin conditions and dual stratifications

M. Nasir[1], M. Waqas[2,*], **O. Anwar Bég[3]**, N. Zamri[4], **Henry J. Leonard[3]** and Kamel Guedri[5]

[1]*Faculty of Informatics and Computing, University Sultan Zainal Abidin (Kampus Gong Badak), Kuala Terengganu, Terengganu 21300,* ***Malaysia***

[2]*NUTECH School of Applied Science and Humanities, National University of Technology, Islamabad 44000,* ***Pakistan***

[3]*Multi-Physical Engineering Sciences Group, Mechanical Engineering, School of Science, Engineering and Environment (SEE), Salford University, Manchester, M54WT,* ***UK.***

[4]*Faculty of Informatics and Computing, University Sultan Zainal Abidin (Besut Campus), Besut, Terengganu 22000,* ***Malaysia***

Mechanical Engineering Department, College of Engineering and Islamic Architecture, Umm Al-Qura University,(kmguedri@uqu.edu.sa), P.O. Box 5555, Makkah 21955, ***Saudi Arabia****.*

**Correspondence:* muhammadwaqas@nutech.edu.pk *(M. Waqas)*

ABSTRACT: A mathematical study is presented to evaluate double stratification effects on the dual convected flow of a non-Newtonian (tangent-hyperbolic) nanoliquids persuaded by porous stretching surface. Thermal radiation along with transpiration (wall suction/injection) and heat source/sink are included. Buongiorno's model is employed for nanoscale effects and a Rosseland diffusion approximation for nonlinear radiative heat transfer. Appropriate similarity transformations are deployed to alter the dimensional governing nonlinear PDEs (partial differential equations) to a nonlinear differential one with physically viable boundary conditions. The transformed dimensionless BVP (boundary value problem) is computed analytically by a HAM (homotopic analysis method) algorithm and a symbolic software. Validation with earlier studies employing the numerical method (Runge-Kutta-Fehlberg) is included. The evolution in velocity, thermal and solutal (nanoparticle) fields are interpreted through graphical outcomes for

the impact of significant sundry parameters. Tabular outcomes are also presented for skin-friction, local Nusselt and Sherwood numbers. A rise in material variable (Weissenberg number), the flow is decelerated while it is accelerated with increasing nonlinear thermal convective parameter, mixed convection parameter and buoyancy ratio values. Temperatures are boosted with increment in radiative, thermophoresis, Brownian motion, thermal Biot number and heat generation parameters whereas they are reduced with increasing thermal stratification parameter. Nanoparticle concentration values are suppressed with higher Schmidt number, Brownian movement and solutal stratification variable however they are boosted with greater values of thermophoresis and concentration Biot number. Local Sherwood number is improved with Schmidt number, concentration stratification parameter and concentration Biot number. Local Nusselt number is strongly increased with greater Prandtl number, thermal stratification number, thermal Biot number and radiative parameter. The study finds applications in thermal nano-polymeric coating flows in materials processing operations.

KEYWORDS: *Heat source/sink; thermal radiation; tangent-hyperbolic nanoliquids; thermal and solutal stratification; suction/ injection; nano-polymeric materials processing.*

1. INTRODUCTION.

Non-Newtonian flows occur in diverse applications in industrial slurry systems [1], polymeric manufacturing technologies [2], biomedical engineering [3] and environmental transport [4]. Examples of such liquids include petrochemical suspensions, coatings, greases, adhesives, lubricants, foodstuffs (milk, chocolate, toffee, syrups), pharmaceutical and biotechnological liquids (linctuses, cough mixtures, sterilization liquids), physiological fluids (blood, synovial lubricant, digestive liquids), river sediments, muds and volcanic lava. Such fluids exhibit an astonishing range of rheological characteristics including shear-thinning (pseudoplasticity), shear-thickening (dilatancy), viscoplasticity, viscoelasticity, microstructural effects, spurting phenomena, stress relaxation, retardation among others. Non-Newtonian fluids therefore produce significant deviation from the classical Newtonian viscous flow model featured in the Navier-Stokes or boundary layer equations. To accurately simulate non-Newtonian fluids, different mathematical models have been established to describe the shear stress-strain characteristics and these generally can be categorized as integral, differential or rate-type models.

Excellent reviews of many such models have been provided by Schowalter [5] and Bird *et al.* [6] and popular non-Newtonian constitutive models include the Maxwell upper convected viscoelastic model, Carreau shear thinning model, Casson viscoplastic model. However presently no model exists which can describe the full range of rheological behaviour encountered in real liquids such as polymers. In a number of materials fabrication operations, polymers are stretched along a vertical plane and this procedure is often accompanied with heat transfer. Stretching rate may be linear or nonlinear e.g. quadratic, exponential etc. An excellent appraisal of the boundary layer analysis of such flows has been provided by Jaluria [7] in which non-Newtonian characteristics have also been shown to exert a considerable impact on momentum along with thermal diffusion. The simple but robust non-Newtonian model known as the *tangent-hyperbolic model* [5] has been shown to be particularly adept at simulating the actual shear characteristics of a variety of polymers. This model is valid for both lower and higher shear rates and is of the "rate type" and furthermore includes properties of relaxation and retardation times which are known to be important in polymer dynamics. This model is a two-parameter non-Newtonian model which features a power-law index and also a material parameter for viscoelastic effects. At high shear polymers become "thinner" and viscosity effects are reduced leading to shear-thinning (thixotropic) behaviour. Shear-thickening is the opposite behaviour to this where greater viscosity is produced and under high pressure, molecules in a polymer crowd together and offer greater resistance to flow. These phenomena can be simulated with the hyperbolic-tangent model. This rheological model has therefore been deployed extensively in recent years to address a wide spectrum of thermal polymeric flows and also other applications in process mechanical engineering and chemical engineering [8-11].

In the 21st century *nanotechnology* has emerged as a major frontier in engineering and materials processing systems. Many new materials have been synthesized by doping existing media with particles having sizes less than 100nm, known as nanoparticles. Engineered at the nano-scale, they achieve substantially improved properties due to their small sizes and have enabled a new generation of materials to be developed with enhanced mechanical, optical, thermal and magnetic properties. A sub-branch of nanomaterials deployed in thermal engineering are known as *nanofluids*, which were introduced by Choi [12]. These are produced by adjourning metallic/non-metallic nano-particles in a base liquid and the subsequent colloidal suspension attains dramatically enhanced heat transmission properties, largely due to the boost in thermal

conductivity but also due to modifications in viscosity. Nanofluids perform significantly more effectively than conventional fluids such as polymers gels, water and air. They also achieve improved cooling properties in a variety of technologies since the base fluid thermal characteristics improve due to nanoparticles [13]. Nanofluids have therefore been embraced widely in biomedical, automotive, environmental, aerospace, marine renewables and also energy engineering. Some popular applications include fuel cells, microelectronics, hybrid power engines and more recently, nano-polymers etc. Nano-polymers [14] are nanostructured polymers and are produced by doping existing polymers with nanoparticles. The nanostructure determines important modifications in the intrinsic properties and via the deployment of different nanoparticles (e.g. metallic spheres, carbon nanotubes etc), nano-polymers have been produced with improved adsorption and stability, wettability adjustment, interfacial tension decline and suspension stability, and more consistent rheology. Nano-polymers require the simultaneous consideration of rheology and nanoscale effects. Buongiorno's two component nanofluid model offers an excellent platform for analyzing thermophoretic, Brownian motion, thermal diffusion and also species diffusion (mass transfer) in such liquids. Experimental studies have confirmed that many nano-polymers show shear-thinning characteristics [15-19] which can be manipulated by percentage doping (volume fraction) and the hyperbolic-tangent non-Newtonian model approximates quite well the behaviour of such liquids. Significant attention has therefore been stimulated in recent years toward modelling nanofluids and nano-polymers with a amalgamation of Buongiorno model and hyperbolic-tangent model. Such investigations require advanced numerical or very powerful analytical methods owing to the inherent nonlinearity of the boundary value problems arising in viscous nano-polymer fluid dynamics. Important analyses in this direction include Atif *et al.* [20] who studied the unsteady thermosolutal hyperbolic-tangent nanofluid flow from a two-dimensional wedge with convective wall heating. They deployed a numerical shooting scheme and showed that temperatures are strongly elevated with Biot number, Weissenberg number, Brownian and thermophoretic parameters. Salahuddin *et al.* [21] computed the boundary-layer flow of hyperbolic-tangent nanoliquid in stagnation flow on a moving cylinder, observing that the flow is decelerated with greater material variable (Weissenberg number) and power-law index while with an increment in stretching rate there is a boost in local Nusselt and Sherwood numbers. Further analyses include Shahzad *et al.* [22] (on reactive magnetized hyperbolic-tangent nanofluid flow from a stretching sheet), Shafiq *et al.* [23] (on magnetic hyperbolic-tangent nanofluid flow with micro-organisms

along an exponentially stretching vertical surface) and Basha *et al*. [24] (on thermodynamic analysis of hyperbolic-tangent nano-polymeric enrobing flow of a circular cylinder). Kumaran *et al.* [25] examined numerically the hydromagnetic bioconvection of hyperbolic-tangent nanopolymer in reactive coating flow on a cylinder in a permeable regime with thermal relaxation effects. Entropy optimized hyperbolic-tangent nanoliquid dual convective reactive flow capturing activation energy is inspected by Awais et al. [26]. Makinde et al. [27] evaluated electrically conducting nanoliquid radiative-reactive flow confined by nonlinear elongating surface. Porous medium significance in magneto-nanoliquid reactive flow under solar radiation is modelled by Eid et al. [28]. Mahanthesh et al. [29] explored three-dimensional nanoliquid slip flow by stretchable nonlinear elongating surface. Boundary-layer magnetized viscoelastic nanoliquid subjected to a stagnation-point is visualized by Narayana et al. [30].

The above studies neglected dual stratification effects. Double stratification arises owing to temperature and concentration variations, respectively in thermosolutal transport. It is important in thermal energy storage systems and also coating dynamics of metallic components e. g. copper tubing, aerospace parts and solar collectors, and modifies the thermal and solutal buoyancy forces acting. Doubly stratified flows also arise in geophysical fluid mechanics including solar ponds, lakes and oceanic circulation. A number of researchers have appraised the effects of dual (thermal/solutal) stratification in nanofluid flows of relevance to materials processing. Ibrahim and Makinde [33] analyzed the impact of dual stratification on boundary-layer flow and heat-transfer induced considering nanoliquid by vertical surface. They showed that local Nusselt and Sherwood numbers are depleted with an increment in thermal and solutal stratification parameters whereas the skin-friction coefficient is boosted with solutal stratification parameter and reduced with thermal stratification parameter. Farooq *et al.* [34] analyzed the phase change stagnation nanofluid flow with double stratification from a nonlinear stretching surface of variable thickness. They witnessed that both thermal and solutal values diminish with increasing stratified (thermal and solutal) parameters. Rehman *et al.* [35] reviewed the consequence of dual stratifications in viscoplastic Casson liquid flow with chemical reactions. Ahmad *et al.* [36] considered the role of double stratification considering chemically reactive squeezing Sutterby flow under mixed convection. Shah *et al.* [37] studied free convective external boundary-layer flow persuaded by vertical cylinder in heat flux damping with double stratification. Ijaz and Ayub [38] scrutinized the influence of heat and mass stratifications for Walter–B viscoelastic flow induced by extending

permeable sheet with generalized heat-mass fluxes. Further investigations of dual stratification include Mallawi *et al.* [39] (for Reiner-Rivlin second grade viscoelastic flow along a Riga plate sensor with thermal and solutal relaxation effects) and Tlili *et al*. [40] (for bioconvective micropolar nanofluid slip flow with the homotopy analysis method). These analyses established the marked modifications in momentum along with heat-mass transfer features computed through inclusion of thermal and solutal stratification effects.

In various thermal polymeric coating systems, a heat source/sink is also utilized to provide a thermal mechanism for modifying transport characteristics and modifying heat-mass transport rates to the boundary e. g. the engineering substrate being coated [7]. Heat generation or absorption also influence the rate of particle deposition in nuclear fuel, electronic chips, and rocket engine systems. While it is challenging to model internal heat generation or absorption, simpler mathematical models can be used for most physical conditions to express their overall characteristics. Heat generation/absorption have therefore also been studied for nanofluid coating dynamics problems in recent years. Ali *et al.* [41] used shooting scheme to simulate the magnetized non-Newtonian nanoliquid flow on an inclined stretched cylinder subjected to heat absorption/generation, witnessing a strong increase in thermal boundary-layer thickness subjected to larger heat generation and the contrary behavior with greater heat absorption. Goud [42] studied the impact of heat generation/absorption in magnetized micropolar rheological flow from a stretching vertical porous surface with thermal radiation and variable wall suction/injection. Further investigations of heat generation/absorption effects in the context of materials processing include Bég *et al.* [43] (for transient magnetized nanofluid slip in porous media), Irfan and Farooq [44] (for hydromagnetic flow from an exponentially stretching sheet in porous media with radiative flux) and Bég *et al.* [45] (for thermocapillary magnetic materials processing in enclosures).

Review of aforesaid studies has revealed that thusfar no investigations have been described which consider simultaneously the *double stratification and heat absorption/generation effects in mixed convection boundary layer flow of hyperbolic-tangent nanofluids from a stretching porous surface with radiative heat transfer*. This regime is of considerable importance in higher temperature materials processing of nano-polymers [46]. This is the emphasis and originality of curent study. Other studies have used the Oldroyd-B fluid model [47] or second grade viscoelastic model [48] or Cross model [49], viscous models [50, 51] *not the tangent hyperbolic shear-thinning*

model. Buongiorno's nanoscale model is deployed and additionally a Rossseland radiative diffusion flux model is implemented. The effects of wall suction/injection, Brownian motion and thermophoresis are also included in the present study as are thermo/solutal convective wall boundary conditions. The re-framed ordinary differential dimensionless boundary value problem is solved with a semi-analytical technique known as the homotopic analysis method (HAM) [52]. Validation with previous numerical studies ignoring dual stratification is included [53]. Convergences of the achieved results are verified in HAM. The evolution in velocity, temperature and concentration (nanoparticle) are illustrated graphically for impact of selected variables including Weissenberg number, power-law rheological index, nonlinear thermal convective parameter, mixed convection parameter, thermal to species buoyancy, radiative, thermophoresis, Brownian motion, thermal Biot number, solutal Biot number, heat source, thermal stratification, solutal stratification and also wall suction/injection parameters. Tables are also presented for skin-friction and local Nusselt and Sherwood numbers. The present study finds applications in nano-polymer film coatings for aerospace and electronics devices [54].

2. MATHEMATICAL MODEL

Steady-state, incompressible and laimar two-dimensional mixed convection boundary-layer of a tangent-hyperbolic nano-polymer from a stretched vertical permeable surface subject to radiative heat transfer and thermo-solutal buoyancy effects is considered. Double (thermal and concentration) stratification effects are included as is heat generation/absorption. Via the adoption of Buongionro's nanoscale model, diffusion of nanoparticles, thermophoresis and Brownian dynamics are included. Convective boundary conditions are assumed at the wall for both the temperature and the nanoparticle concentration. The nano-polymer is assumed to be optically thick, gray and absorbing and emitting but non-scattering, allowing the deployment of the Rosseland diffusion flux model which provides a good approximation for such cases. The vertical sheet (see **Fig. 1**) is stretched with a linear velocity $u_w(x) = cx$ where c is a dimensional constant. The governing boundary layer governing equations for the stratified nano-polymer flow may be expressed as [8]:

$$\frac{\partial u}{\partial x}+\frac{\partial v}{\partial y}=0, \tag{1}$$

$$u\frac{\partial u}{\partial x}+v\frac{\partial v}{\partial y}=\upsilon\left(1-\lambda\right)\frac{\partial^2 u}{\partial y^2}+g\left\{\Lambda_3\left(C-C_\infty\right)+\Lambda_4\left(C-C_\infty\right)^2\right\}+\sqrt{2}\upsilon\Gamma\lambda\left(\frac{\partial u}{\partial y}\right)\frac{\partial^2 u}{\partial y^2}- \\ +g\left\{\Lambda_1\left(T-T_\infty\right)+\Lambda_2\left(T-T_\infty\right)^2\right\}, \tag{2}$$

$$u\frac{\partial T}{\partial x}+v\frac{\partial T}{\partial y}=\alpha\frac{\partial^2 T}{\partial y^2}+\frac{16\sigma^* T_\infty^3}{3k^*\left(\rho c\right)_f}\frac{\partial^2 T}{\partial y^2}+\frac{Q_0}{\left(\rho c\right)_f}\left(T-T_\infty\right)+ \\ +\tau\left[D_B\frac{\partial C}{\partial y}\frac{\partial T}{\partial y}+\frac{D_T}{T_\infty}\left(\frac{\partial T}{\partial y}\right)^2\right], \tag{3}$$

$$u\frac{\partial C}{\partial x}+v\frac{\partial C}{\partial y}=\frac{D_T}{T_\infty}\frac{\partial^2 T}{\partial y^2}+D_B\frac{\partial^2 C}{\partial y^2}, \tag{4}$$

The boundary conditions assumed at wall and in the free stream (edge of the boundary-layer coating regime) are given as:

$$\text{at } y=0,\ u=u_w\left(x\right)=cx,\ v=-v_w,-D_B\frac{\partial C}{\partial y}=h_g\left(C_f-C\right),-k\frac{\partial T}{\partial y}=h_f\left(T_f-T\right), \tag{5}$$

$$\text{when } y\to\infty,\ u\to 0,\ C\to C_\infty=C_0+d_2x,\ T\to T_\infty=T_0+d_1x. \tag{6}$$

Here $\upsilon\left(=\dfrac{\mu}{\rho_f}\right)$ represents the kinematic viscosity, ρ_f is nanoliquid density, $\alpha=\dfrac{k}{\left(\rho c\right)_f}$ for thermal diffusivity, λ a tangent-hyperbolic material (non-Newtonian) power-law index, g is gravitational acceleration, Γ is the tangent-hyperbolic material constant, $\left(\Lambda_1,\Lambda_3\right)$ for linear (thermal, concentration) expansion coefficients, μ for dynamic viscosity, $\tau=\dfrac{\left(\rho c\right)_p}{\left(\rho c\right)_f}$ are heat capacity ratio with $\left(\rho c\right)_f$ for nanofluid heat capacity, $\left(\Lambda_2,\Lambda_4\right)$ for nonlinear (thermal,

concentration) expansion coefficients, $(\rho c)_p$ for nanoparticles adequate heat capacity, (c, d_1, d_2) for dimensional constants, Q_0 denotes the coefficient of heat absorption/generation, σ^* is the Stefan-Boltzmann radiation constant, (D_T, D_B) for (thermophoresis, Brownian) diffusion coefficients, k^* for the coefficient of mean absorption, (T, C) denote nanofluid temperature, concentration respectively, $(u_w(x), v_w)$ for (stretching, suction/injection) velocity respectively.

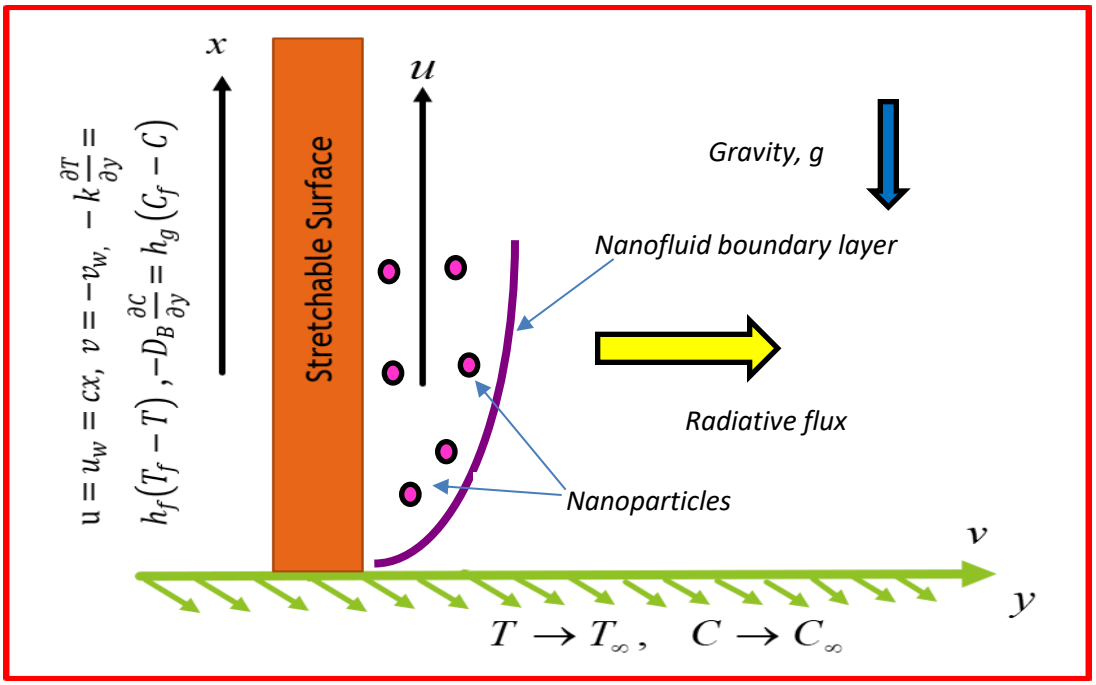

Fig. 1. Physical model for thermo/solutal stratified radiative nano-polymer flow

k denotes nanofluid thermal conductivity, (h_f, h_g) for are the wall convective heat and mass transfer coefficients, (T_∞, C_∞) for ambient liquid (temperature, concentration) respectively, (T_0, C_0) for reference (temperature, concentration) respectively. $(T_f = T_0 + a_1 x, C_f = C_0 + a_2 x)$ for the thermal and solutal stratification (temperature, concentration) respectively and (u, v) for components of velocity in the (x, y) direction, respectively. The partial differential boundary value

problem defined by Eqns. (1)-(6) is formidable to solve even with powerful numerical methods. It is therefore judicious to invoke the following similarity transformations:

$$\eta = y\sqrt{\frac{c}{\upsilon}},\ v = -\sqrt{c\upsilon}\, f(\eta),\ u = cxf'(\eta),\ \phi(\eta) = \frac{C - C_\infty}{C_f - C_0},\ \theta(\eta) = \frac{T - T_\infty}{T_f - T_0}. \tag{7}$$

Implementing in Eqns. (1)-(6), Eq. (1) i. e. mass conservation is satisfied automatically, whereas Eqns. $(2)-(6)$ are transformed to the following ordinary differential boundary layer equations with transformed boundary conditions at the wall and in the free stream:

$$(1-\lambda) f''' + f\ f'' + \lambda We\, f''\, f''' - f'^2 + \delta\left[N(1+\beta_c\phi)\phi + (1+\beta_t\theta)\theta\right] = 0, \tag{8}$$

$$\left(\frac{4}{3}R + 1\right)\theta'' + \Pr\left(f\theta' - f'\theta\right) + \Pr\left(-S_1 f' + S\theta + N_t\theta'^2 + N_b\phi'\theta'\right) = 0, \tag{9}$$

$$\phi'' + Sc\left(f\phi' - f'\phi\right) + \frac{N_t}{N_b}\theta'' - Sc\, S_2 f' = 0, \tag{10}$$

$$\begin{cases} \text{at } \eta = 0,\ f = h,\ f' = 1,\ \phi' = -\gamma_2\left(1 - S_2 - \phi(\eta)\right),\ \theta' = -\gamma_1\left(1 - S_1 - \theta(\eta)\right), \\ \text{as } \eta \to \infty,\ f' \to 0,\ \phi \to 0,\ \theta \to 0\ . \end{cases} \tag{11}$$

Here $(')$ signifies differentiation for η, λ is the tangent hyperbolic non-Newtonian power-law index parameter, *We* is Weissenberg number (ratio of elastic to viscous hydrodynamic force), δ is mixed convection variable, Gr_x for local thermal Grashof number i.e. thermal buoyancy parameter, N denotes the ratio of concentration to thermal buoyancy forces, Gr_x^* is local solutal (nanoparticle species) Grashof number i.e. local solutal (concentration) buoyancy parameter, (β_t, β_c) are nonlinear (thermal, concentration) convection parameters, N_t is thermophoresis variable, (S_1, S_2) are (thermal, concentration/solutal) stratification parameters, Pr is Prandtl number, N_b is Brownian motion parameter, R is radiation-conduction parameter, S is the heat

generation/absorption i.e. heat source/sink parameter, Sc represents Schmidt number (ratio of momentum and nanoparticle diffusivities), (γ_1, γ_2) are (thermal, concentration) Biot numbers and h is the wall transpiration parameter (for the permeable stretching surface) wherein for suction $(h>0)$ and injection $(h<0)$. These quantities take the following definitions:

$$
\begin{aligned}
&We=\frac{\sqrt{2}}{\sqrt{\upsilon}}\Gamma c^{\frac{3}{2}}x,\ \delta=\frac{Gr_x}{\mathrm{Re}_x^2},\ Gr_x=\frac{g\Lambda_1\left(T_f-T_0\right)x^3}{\upsilon^2},\ \mathrm{Gr}_x^*=\frac{g\Lambda_3\left(C_f-C_0\right)x^3}{\upsilon^2},\\
&\beta_t=\frac{\Lambda_2\left(T_f-T_0\right)}{\Lambda_1},\ \beta_c=\frac{\Lambda_4 C_\infty}{\Lambda_3},\ N=\frac{Gr_x^*}{Gr_x},\ \mathrm{Re}_x=\frac{xu_w}{\upsilon},\ h=\frac{v_w}{\sqrt{c\upsilon}},\\
&N_t=\frac{\tau D_T\left(T_f-T_0\right)}{T_\infty\upsilon},\ S_1=\frac{d_1}{a_1},\ S_2=\frac{d_2}{a_2},\ \mathrm{Pr}=\frac{\upsilon}{\alpha},\ N_b=\frac{\tau D_B\left(C_f-C_0\right)}{\upsilon},\\
&R=\frac{4\sigma^*T_\infty^3}{kk^*},\ S=\frac{Q_0}{\left(\rho c\right)_f c},\ Sc=\frac{\upsilon}{D_B},\ \gamma_1=\frac{h_f}{k}\sqrt{\frac{\upsilon}{c}},\ \gamma_2=\frac{h_g}{D_B}\sqrt{\frac{\upsilon}{c}}.
\end{aligned}
\tag{12}
$$

In nanomaterials processing, important gradients of the key variables (velocity, temperature and concentration) at the wall are the skin–friction coefficient and local (Nusselt, Sherwood) numbers (C_{fx}, Nu_x, Sh_x). These are defined respectively as:

$$
C_{fx}=\frac{2\tau_w}{\rho u_w^2},\ \tau_w=\mu\left(\left(1-\lambda\right)\frac{\partial u}{\partial y}+\lambda\frac{\Gamma}{\sqrt{2}}\left(\frac{\partial u}{\partial y}\right)^2\right)_{y=0},
\tag{13}
$$

$$
Nu_x=-\frac{xq_w}{k\left(T_f-T_\infty\right)},\ q_w=-\left(k+\frac{16\sigma^*T_\infty^3}{3k^*}\right)\left(\frac{\partial T}{\partial y}\right)_{y=0},
\tag{14}
$$

$$
Sh_x=-\frac{xq_m}{D_B\left(C_f-C_\infty\right)},\ q_m=-D_B\left(\frac{\partial C}{\partial y}\right)_{y=0}.
\tag{15}
$$

The coefficient of skin–friction along with local Nusselt and Sherwood numbers are expressed in simple (non-dimensional) form based on the similarity variables in Eqn. (7) as:

$$
C_{fx}\,\mathrm{Re}_x^{-\frac{1}{2}}=\frac{\lambda}{2}We\left(f''(0)\right)^2+\left(1-\lambda\right)f''(0),
\tag{16}
$$

$$Nu_x \,\mathrm{Re}_x^{-\frac{1}{2}} = -\frac{\left(\frac{4}{3}R+1\right)}{1-S_1}\theta'(0), \tag{17}$$

$$Sh_x \,\mathrm{Re}_x^{-\frac{1}{2}} = -\frac{1}{1-S_2}\phi'(0). \tag{18}$$

3. HOMOTOPY ANALYSIS METHOD COMPUTATIONS AND CONVERGENCE STUDY

The nonlinear differential Eqns. $(8)-(10)$ are simplified and solved for the third order of velocity $f(\eta)$, second–order of temperature $\theta(\eta)$, and second-order concentration $\phi(\eta)$. We follow the homotopic procedure proposed by Liao [52] for the solution of these ordinary differential equations with associated boundary conditions. Although algebraically rigorous, HAM [56-58] is a very versatile procedure using power series expansions which has found considerable popularity in non-Newtonian fluid dynamics. HAM can accommodate any order or degree of nonlinear differential equation systems and also very complex boundary conditions. In the present simulations, the initial guesses $(f_o,\ \theta_o,\ \phi_o)$, along with their linear operatives $(L_f,\ L_\theta,\ L_\phi)$ for the dimensionless momentum, energy, and concentration boundary layer equations of the nanopolymer stretching flow i. e. Eqns. (8)-(10), are defined as:

$$f_0(\eta) = h + \left(1-e^{-\eta}\right),\ \theta_0(\eta) = \left(\frac{\gamma_1}{1+\gamma_1}\right) * (1-S_1)e^{-\eta},\ \phi_0(\eta) = \left(\frac{\gamma_2}{1+\gamma_2}\right) * (1-S_2)e^{-\eta}, \tag{19}$$

These initial guesses are associated with:

$$L_f = f''' - f',\ L_\theta = \theta'' - \theta,\ L_\phi = \phi'' - \phi, \tag{20}$$

These expressions satisfy the subsequent conditions:

$$\left.\begin{aligned} L_f\left(C_1 + C_2 e^{\eta} + C_3 e^{-\eta}\right) = 0,\ L_\theta\left(C_4 e^{\eta} + C_5 e^{-\eta}\right) = 0, \\ L_\phi\left(C_6 e^{\eta} + C_7 e^{-\eta}\right) = 0, \end{aligned}\right\} \tag{21}$$

Here $C_i\ (i = 1-7)$ specify the subjective constants.

In HAM, ensuring the convergence of results is necessary. The assisting parameter shows an animated character to monitor and modify the convergence region of the power series solution.

We have mapped the h–curves in **Fig. 2**. It is observed that optimized values of $\hbar_f, \hbar_\theta$ and $\hbar_\phi$ in Figs. 2 and 3 are $-2.0 \le \hbar_f \le -0.2$, $-1.9 \le \hbar_\theta \le -0.1$ and $-1.9 \le \hbar_\phi \le -0.1$

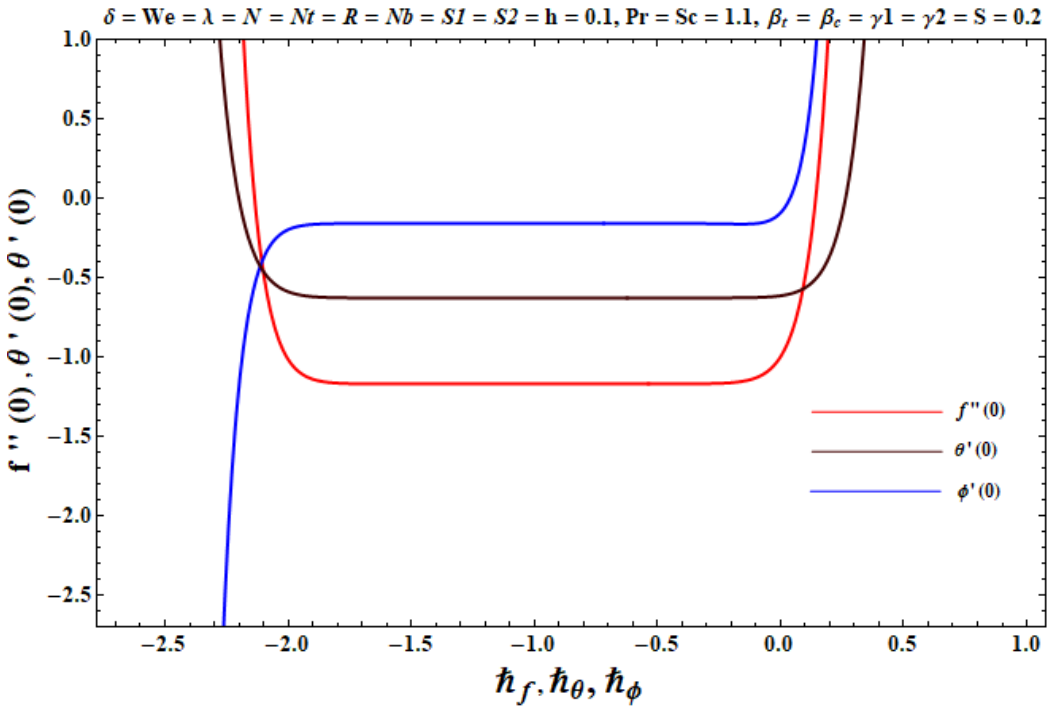

Fig. 2. $\hbar$–curve impression on $f''(0)$, $\theta'(0)$ and $\phi'(0)$.

Table 1 describes the convergence of series solution for the diverse order of approximation. It is verified that momentum, energy, and concentration equations converge at the 30th order of approximations. This is prescribed therefore in all subsequent analysis.

Table 1. HAM convergence of sequence solutions for the diverse order of approximations when $\lambda = We = \delta = S = N_t = N_b = N = R = S_1 = S_2 = 0.1$, $\Pr = Sc = 1.1$ and $\beta_t = \beta_c = \gamma_1 = \gamma_2 = h = 0.2$.

Order of approximations	$-f''(0)$	$-\theta'(0)$	$-\phi'(0)$
1	*1.1449*	*0.1599*	*0.1507*
5	*1.1715*	*0.1600*	*0.1462*
10	*1.1718*	*0.1600*	*0.1463*
15	*1.1718*	*0.1600*	*0.1463*
20	*1.1718*	*0.1600*	*0.1463*

25	*1.1718*	*0.1600*	*0.1463*
30	*1.1718*	*0.1600*	*0.1463*

4. HAM RESULTS AND DISCUSSION

Comprehensive graphical visualizations of the influence of all key variables on transport aspects have been presented in **Figs. 3-20** and **Tables 2-5**.

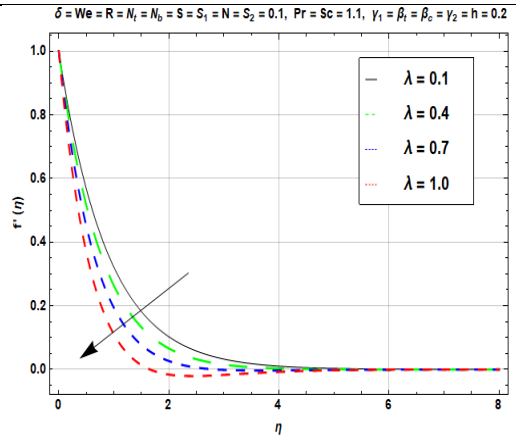

Fig. 3. λ impression on $f'(\eta)$.

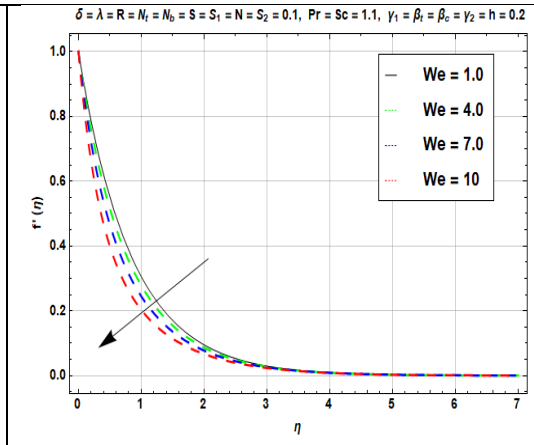

Fig. 4. *We* impression on $f'(\eta)$.

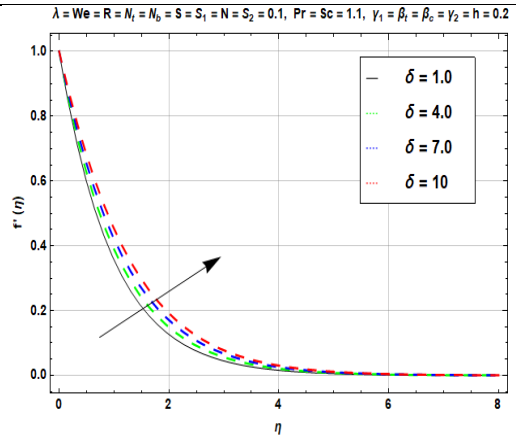

Fig. 5. δ impression on $f'(\eta)$.

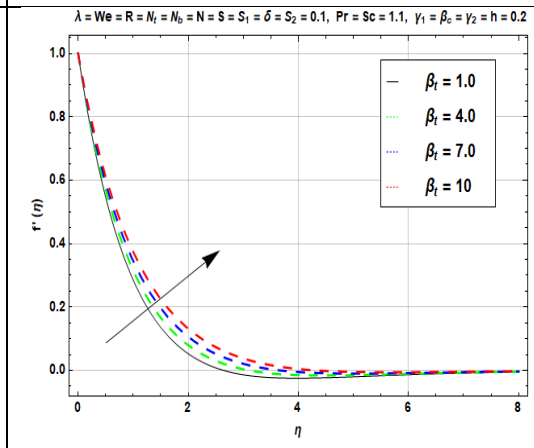

Fig. 6. β_t impression on $f'(\eta)$.

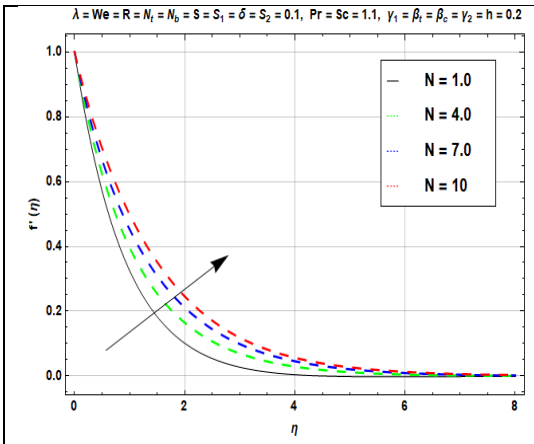

Fig. 7. N impression on $f'(\eta)$.

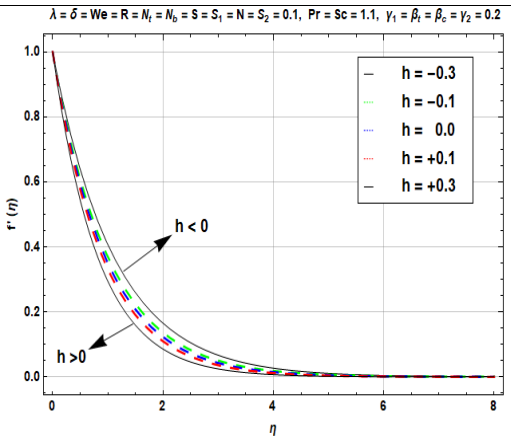

Fig. 8. h impression on $f'(\eta)$.

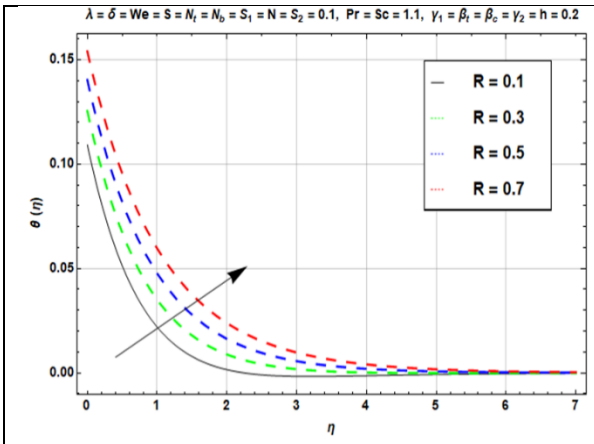

Fig. 9. R impression on $\theta(\eta)$.

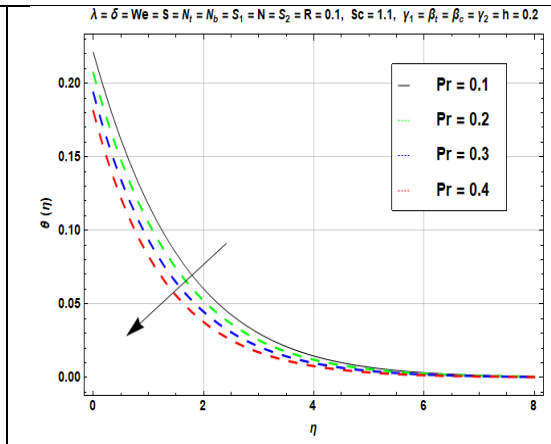

Fig. 10. Pr impression on $\theta(\eta)$.

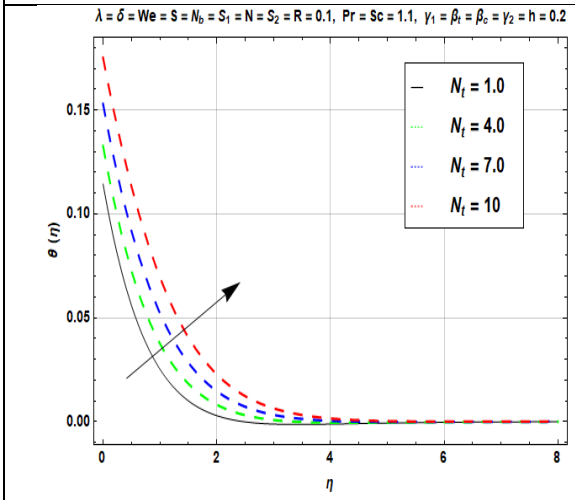

Fig. 11. N_t impression on $\theta(\eta)$.

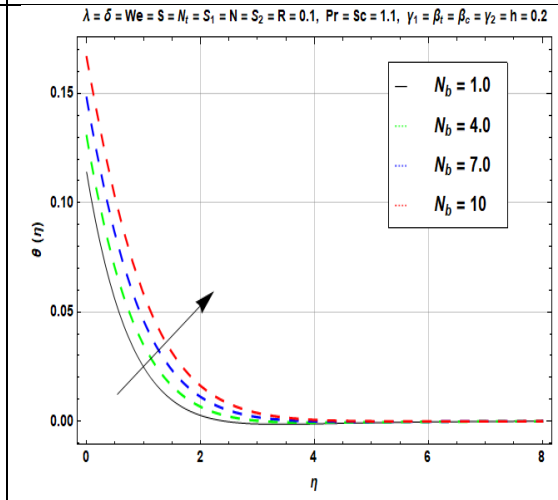

Fig. 12. N_b impression on $\theta(\eta)$.

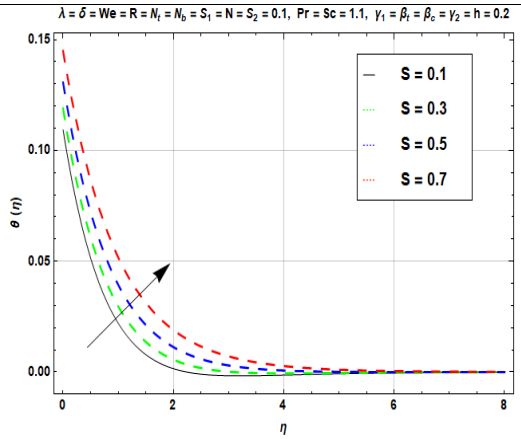

Fig. 13. S impression on $\theta(\eta)$.

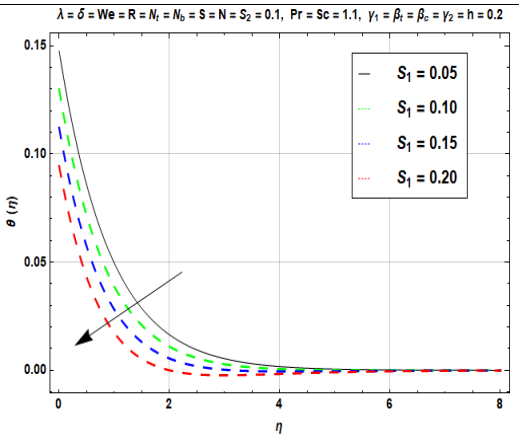

Fig. 14. S_1 impression on $\theta(\eta)$.

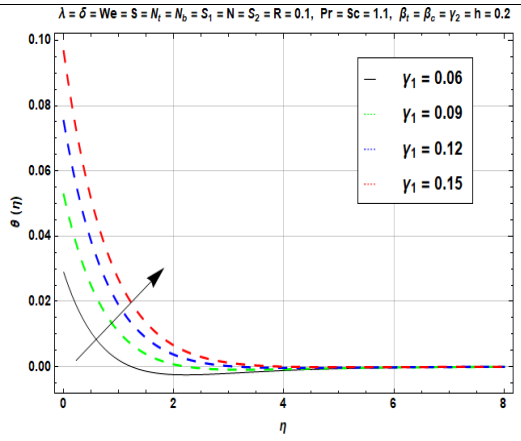

Fig. 15. γ_1 impression on $\theta(\eta)$.

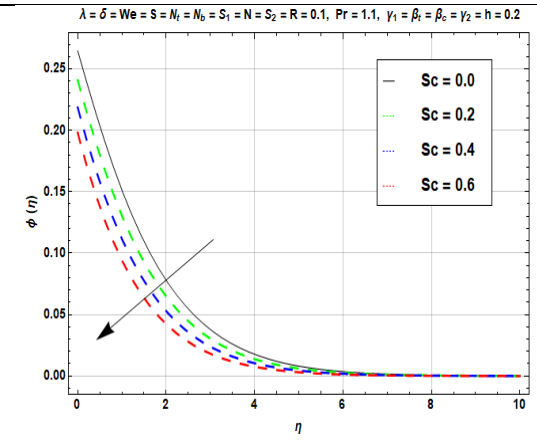

Fig. 16. Sc impression on $\phi(\eta)$.

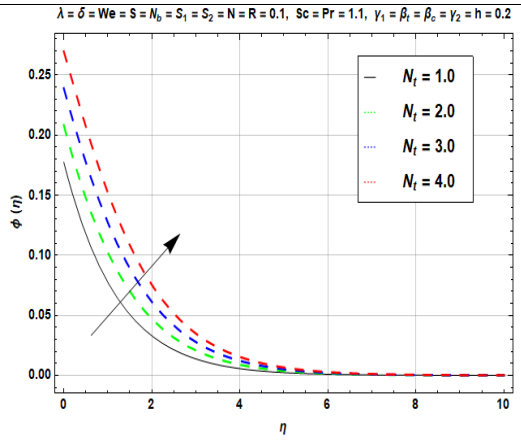

Fig. 17. N_t impression on $\phi(\eta)$.

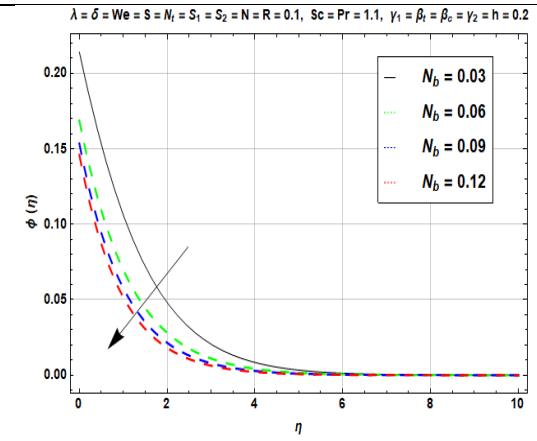

Fig. 18. N_b impression on $\phi(\eta)$.

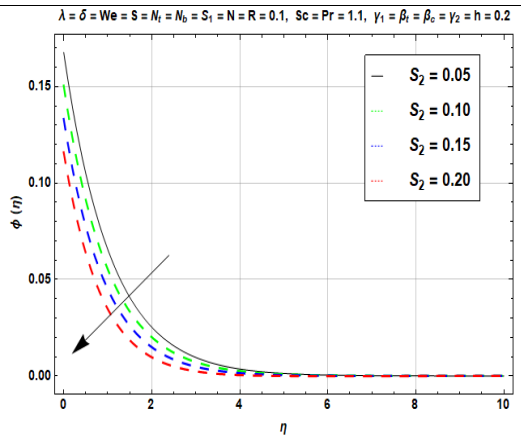

Fig. 19. S_2 impression on $\phi(\eta)$.

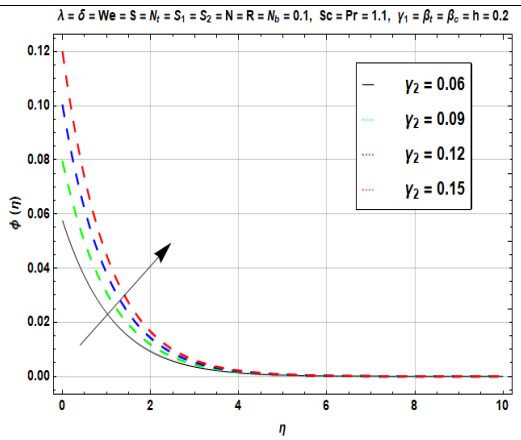

Fig. 20. γ_2 impression on $\phi(\eta)$.

Table 2. Skin friction $C_{fx}\,\mathrm{Re}_x^{-\frac{1}{2}}$ for selected parameters when $\mathrm{Pr} = Sc = 1.1$, $S = N_t = N_b = R = S_1 = S_2 = 0.1$ and $\beta_t = \beta_c = \gamma_1 = \gamma_2 = h = 0.2$.

λ	We	δ	N	$C_{fx}\,\mathrm{Re}_x^{-\frac{1}{2}}$
0.2	0.1	0.1	0.1	-0.9904
0.3				-0.9287
0.4				-0.8611
0.1	0.2			-1.0455
	0.3			-1.0432
	0.4			-1.0409
	0.1	0.2		-1.0438
		0.3		-1.0398
		0.4		-1.0357
		0.1	0.2	-1.0469
			0.3	-1.0460
			0.4	-1.0451

Table 3. Nusselt number $Nu_x\,\mathrm{Re}_x^{-\frac{1}{2}}$ for selected parameters when $\lambda = We = \delta = S = N = S_2 = 0.1$, $Sc = 1.1$, $\beta_t = \beta_c = \gamma_2 = h = 0.2$.

Pr	R	N_b	N_t	S_1	γ_1	$Nu_x\,\mathrm{Re}_x^{-\frac{1}{2}}$

1.2	0.1	0.1	0.1	0.1	0.2	0.2037
1.3						0.2056
1.4						0.2072
1.1	0.2					0.2219
	0.3					0.2419
	0.4					0.2613
	0.1	0.2				0.2013
		0.3				0.2012
		0.4				0.2010
		0.1	0.2			0.2013
			0.3			0.2012
			0.4			0.2010
			0.1	0.2		0.2175
				0.3		0.2379
				0.4		0.2649
				0.1	0.3	0.2787
					0.4	0.3448
					0.5	0.4019

Table 4. Sherwood number $Sh_x \operatorname{Re}_x^{-\frac{1}{2}}$ for selected parameters when $\lambda = We = \delta = S = N = R = S_1 = 0.1,\ \Pr = 1.1, \beta_t = \beta_c = \gamma_1 = h = 0.2.$

Sc	S_2	N_b	N_t	γ_2	$Sh_x \operatorname{Re}_x^{-\frac{1}{2}}$
1.2	0.1	0.1	0.1	0.2	0.1654
1.3					0.1679
1.4					0.1701
1.1	0.2				0.1734
	0.3				0.1872
	0.4				0.2057
	0.1	0.2			0.1719
		0.3			0.1750
		0.4			0.1765
		0.1	0.2		0.1441
			0.3		0.1257
			0.4		0.1074
			0.1	0.3	0.2272
				0.4	0.2836
				0.5	0.3332

Table 5. Comparison outcomes of $-f''(0)$ considering $\delta = N = h = \beta_t = \beta_c = \gamma_1 = \gamma_2 = 0$.

λ	We	Ref. [58]	Present study
0.0	0.0	1.0000	1.00000
0.1	0.0	0.9491	0.94868
0.2	0.0	0.8944	0.89443
0.0	0.3	1.00000	1.00000
0.1	0.3	0.9432	0.94248
0.2	0.3	0.8805	0.88023
0.0	0.5	1.00000	1.00000
0.1	0.5	0.9380	0.93826

All data has been selected to represent as accurately as possible real nano-polymers and is extracted from Das *et al.* [13] for nanoscale properties, Chen *et al.* [17] for rheological characteristics, and Atif *et al.* [20] and Farooq *et al.* [34] for convective heating and double stratification parameters.

Figs 3–8 illustrate the impact of λ, *We*, h, δ, β_t and N on velocity (f'). In Figure 3, it is witnessed that augmentation in λ induces a strong decline in $f'(\eta)$. Clearly λ appears in Eqn. (8), i.e. in the terms $(1-\lambda)f''', +\lambda We f'' f'''$. As λ increases from less than 1 to a value of 1 (Newtonian), the nanopolymer turn out to be less shear-thinning (pseudoplastic) and approaches conventional viscous Newtonian behaviour. This slows the flow and upsurges momentum boundary-layer thickness. The dilatant case for which λ>1 is not considered. Fig. 4 illustrates that with greater (We) there is also a depletion in $f'(\eta)$ i.e. the flow is retarded. In fact We is the relation of fluid's relaxation time and the time scale of the flow. For situations where We is low i.e. 1.0, then the time-scale of a flow is much greater than the relaxation time and the flow is accelerated since the flow is viscous-dominated, not elasticity-dominated (elastic effects relax adequately). Conversely when We is large (4, 7, 10) then the time scale of the elastico-viscous nanopolymer is much lower than the relaxation time and elastic effects dominate which result in a slower response in the boundary layer and the associated deceleration. Weissenberg number features in the single nonlinear term, $, +\lambda We f'' f'''$ in Eqn. (8) and clearly an increase in this important parameter produces a thicker momentum boundary-layer. Analogous findings have been reported in for example Mahantesh *et al.* [9]. Fig. 5 shows that with elevation in the mixed convection parameter (δ), a strong acceleration is induced in the boundary-layer flow. This

parameter arises in the thermal and buoyancy coupling terms in Eqn. (8), viz $\delta[N(1+\beta_c\phi)\phi + (1+\beta_t\theta)\theta]$ and exerts a significant aiding effect on momentum diffusion since both thermal convection currents (buoyancy) and species buoyancy assist the boundary layer development. Velocities are augmented and momentum (hydrodynamic) boundary-layer thickness is decreased on the stretching sheet. Fig. 6 depicts that with greater estimations of thermal stratification parameter (β_t) there is a substantial enhancement in velocity $f'(\eta)$. Again, the thermal stratification aspect is simulated through the improved coupling term $(1+\beta_t\theta)\theta$ in Eqn. (8) which couples the momentum Eqn. (8) with the energy equation (9). $\beta_t = \frac{\Lambda_2(T_f - T_0)}{\Lambda_1}$ which includes a temperature difference. A strong depletion in momentum boundary-layer thickness is therefore produced with greater thermal stratification, associated with an intensification in convection currents, and this has been observed in a number of other investigations also including Ibrahim and Makinde [33] and Rehman *et al.* [35]. Fig. 7 displays that with increment in the thermal to species (solutal) buoyancy ratio, (N) there is an associated elevation in velocity, $f'(\eta)$. $N = \frac{Gr_x^*}{Gr_x}$ and clearly for $N = 1$, both solutal and clearly the species Grashof number $Gr_x^* = \frac{g\Lambda_3(C_f - C_0)x^3}{\upsilon^2}$ and thermal Grashof number $Gr_x = \frac{g\Lambda_1(T_f - T_0)x^3}{\upsilon^2}$ will be equal for this scenario. However, for $N > 1$, solutal buoyancy will dominate thermal buoyancy and this encourages momentum diffusion in the regime. Flow acceleration is generated, and momentum boundary layer thickness is therefore reduced with greater values of N. Fig 8 visualizes the influence of lateral wall mass flux (h) on the velocity field. This effect is simulated in the wall boundary condition (11) i. e. at $\eta = 0, f = h$. For the case of injection i.e. $(h < 0)$, nanopolymer is blown through the permeable sheet into the boundary layer and this assist momentum development, accelerates the flow and decreases momentum boundary layer thickness. Conversely for the case of suction $(h > 0)$ nanofluid is removed from the boundary layer which adheres more tightly to the sheet surface. This destroys momentum, inhibits the flow and increases momentum (hydrodynamic) boundary layer thickness. It is also noteworthy that in all the plots, asymptotically smooth profiles are computed via HAM in the free stream indicating that an adequately large infinity boundary condition has been utilized in the simulations.

Figs.9–15 exhibit the influence of R, Pr, S_1, N_t, S, γ_1, and N_b on $\theta(\eta)$. **Fig. 9** shows that a strong elevation in temperature $\theta(\eta)$ is computed with increment in the radiative conductive parameter (R). This variable features in the thermal diffusion term, $\left(\frac{4}{3}R+1\right)\theta''$ in the thermal boundary layer Eqn. (9). For R = 1 both thermal radiation and thermal conduction modes contribute equally. For R < 1 thermal conduction is dominated by thermal radiation heat flux. For R = 0 radiative flux vanishes. However, the additional radiative flux present with increasing R values (even when less than unity) contributes significantly towards energizing the nanopolymer boundary layer. This results in a boost in temperatures. Thermal boundary-layer thickness is therefore accentuated with greater radiative flux. It is important therefore to include in higher temperature nanomaterials processing the radiative effect since otherwise temperatures are clearly under-predicted and thermal boundary layer thickness is also under-estimated. Analogous observations have been made by Ali *et al.* [41] and Irfan *et al.* [44]. It is also noteworthy that the Rosseland flux approximation is confined to optically thick gray fluids. For more refined estimations of radiative transfer, a more complex model such as the Schuster-Schwartzchild two-flux approximation or the Trauggot P1 differential flux approximation [55] is recommended and these may be considered in future studies. Fig. 10 displays that with rise in Pr there is a marked decrement in $\theta(\eta)$. In fact Pr is contrariwise related to thermal conductivity. For low Pr, thermal conductivity is greater in the nanopolymer whereas for higher Pr it is smaller. This results in a diminution in thermal diffusion relative to momentum diffusion and a plummet in temperatures. Thermal boundary-layer thickness is also suppressed with greater Prandtl number. Fig. 11 displays that with enhancement in the nanoscale thermophoresis parameter (N_t), there is a considerable rise in temperatures in boundary-layer at all estimations of transverse coordinate (η). Besides in the energy Eqn. (9), Nt features in the quadratic temperature term, $+Pr(+N_t\theta'^2)$. It represents the exodus of nano-particles subjected to temperature gradient from a hotter zone in the regime to a colder zone. This effect therefore encourages thermal diffusion and uplifts temperature and also thermal boundary-layer thickness. This trend has been confirmed in numerous nanofluid boundary layer flow studies deploying the Buongiorno model, for illustration, Ray *et al.* [54], among others. Fig. 12 indicates that with greater values of the Brownian motion parameter, (N_b), temperature $\theta(\eta)$ increase. N_b simulates the significant role of random nanoparticle motions in the nano-

polymer and arises in the energy Eqn. (9) via the term $+N_b\phi'\theta'$ which is assistive and is also coupled as expected to the nanoparticle concentration Eqn. (10). Due to increased chaotic nanoparticles movement, the kinetic energy of nanoparticles improves. This boosts the nanofluid and raises temperatures. Thermal boundary-layer thickness is therefore also improved in the stretching sheet regime. It is also noteworthy that increment in Brownian motion will accelerate the random movement which serves to disperse the nanoparticles more throughout the boundary layer and will consequently reduce nanoparticle concentration as described later (Fig. 19). Fig. 13 reveals that increment in heat generation i.e. S >0 produces a strong elevation in temperature, $\theta(\eta)$. The parameter *S* arises only in the single linear term, $S\theta$ in the energy Eqn. (9) but is very impactful on the heat transfer process. The nanopolymer is energized with the surplus thermal energy associated with heat generation (as induced for example with a hot spot in materials processing operations [7]). This enhances thermal boundary layer thickness. Conversely in Fig. 14, it is evident that elevation in the thermal stratification parameter, (S_1) generates the opposite effect to heat generation. Greater thermal stratification inhibits thermal diffusion and the transport of heat in the nanopolymer. This decreases temperatures and depletes thermal boundary layer thickness. This is attributable to the discrepancy between the wall (surface) temperature and the ambient (free stream) temperature, as simulated via S_1. It is also pertinent to note that in the mathematical model studied, S_1 features both in the energy Eqn. (9) in the term $Pr(-S_1 f')$ and also the augmented wall boundary condition $\theta' = -\gamma_1(1 - S_1 - \theta(\eta))$ in Eqn. (11). S_1 therefore exerts a strong role in modifying temperature distributions and if this parameter is neglected the temperature and thermal boundary-layer thickness are over-estimated. A more realistic appraisal of nanopolymeric thermal coating flows therefore requires inclusion of this effect in mathematical models [7]. From inspection of Fig. 15 it is apparent that a strong augmentation in temperature is induced with a rise in thermal Biot number (γ_1). This effect is associated with convective heating at the wall (sheet) and simulated also via the augmented thermal boundary condition in Eqn (11) i.e. $\theta' = -\gamma_1(1 - S_1 - \theta(\eta))$. As (γ_1) is increased there is boost in heat transferred from the wall to the boundary layer which is progressive. This encourages thermal diffusion in the nanopolymer and induces a heating aspect (thicker thermal boundary-layer). Thermal Biot number elaborates the relative significance of thermal conduction and thermal convection heat transfer modes in controlling the temperature distribution through the nanopolymer boundary-layer regime. When

(γ_1) is small, the wall region is dominated by heat conduction which is much speedier than heat convection away from its surface along with thermal gradients are insignificant within this. Thermal Biot number smaller than 0.1 corresponds to "thermally thin" scenarios. For higher values (also shown in Fig. 16), this corresponds to "thermally thick" regimes. Clearly thermal Biot number has a major effect on temperature distribution throughout the boundary layer regime. It is further emphasized that all Figs. 10-15 confirm the prescription of a adequately large infinite boundary condition in the HAM computations, ensuring that the correct temperature distributions are computed.

Figs.16–20 exhibition the role of Sc, S_2, N_t, γ_2, and N_b on $\phi(\eta)$. There is a robust decline in $\phi(\eta)$ with increment in Sc as demonstrated in Fig.16. Higher values of *Sc* imply a lower value of the Brownian diffusion coefficient i.e. molecular diffusivity of the nanoparticles is reduced relative to the momentum diffusivity (*Sc* is the relation of momentum and molecular diffusivity). When *Sc* = 1 then momentum and nanoparticles disseminated at the similar rate and the momentum and species boundary-layer thicknesses are also equal. Maximum concentration is computed for lowest Schmidt number and arises at the wall (η = 0). Concentration boundary-layer thickness is strongly diminished with increment in *Sc*. Figs. 17 and 18 show that as thermophoresis (N_t) parameter is increased, concentration $\phi(\eta)$ is enhanced whereas with greater Brownian motion parameter (N_b) a decrement is computed. Thermophoresis encourages particle migration from hot to cold zones and assists species diffusion producing a greater concentration boundary layer thickness. However Brownian motion leads to a dispersion in nanoparticle distribution due to chaotic motion associated with flow acceleration and reduces concentration boundary-layer thickness. A rise in the solutal stratification parameter (S_2) there is a considerable depletion in concentration magnitudes, $\phi(\eta)$ as witnessed in Fig. 19. The parameter (S_2) appears both in the species boundary-layer Eqn. (11) i.e. in the linear term, $-ScS_2f'$ and also in the modified solutal wall boundary condition in Eqn. (11) i.e. $\phi' = -\gamma_2(1 - S_2 - \phi(\eta))$. It elaborates relative role of convective to molecular diffusion in vicinity of the wall and is therefore a convective mass transfer boundary condition. The increase in difference between surface (wall) concentration and ambient concentration decreases for larger (S_2), which inhibits nanoparticle mass diffusion i.e. lowers

$\phi(\eta)$. Concentration boundary-layer thickness is thus also adversely affected by increasing solutal stratification and this concurs with earlier studies e.g [33]. The effect of elevation in the solutal Biot number (γ_2) as computed in Fig. 20 is to strongly elevate $\phi(\eta)$ i. e. $\phi(\eta)$ is an increasing function of (γ_2). A substantial enhancement in concentration boundary-layer thickness therefore accompanies an escalation in solutal Biot number.

Table 2. expresses the influence of different physical variables on the skin friction coefficient $C_{fx}\,\mathrm{Re}_x^{-\frac{1}{2}}$. It is evident that the skin friction coefficient $C_{fx}\,\mathrm{Re}_x^{-\frac{1}{2}}$ decays with an increment in λ, We, δ and N i.e. higher values of power-law index, Weissenberg number and buoyancy ratio parameter decelerate the flow. Shear stress behaviour at the wall is therefore strongly manipulated by nano-polymer rheological characteristics and buoyancy force interplay, which is critical in materials processing operations. **Table 3**. signifies the impact of several parameters on Nusselt number $Nu_x\,\mathrm{Re}_x^{-\frac{1}{2}}$. It is witnessed that Nusselt number $Nu_x\,\mathrm{Re}_x^{-\frac{1}{2}}$ is increased with enhancing estimations of Prandtl number, radiative parameter, thermal stratification parameter and thermal Biot number i.e. Pr, R, S_1 and γ_1. Heat-transfer to the wall (sheet) is therefore accentuated with increment in these parameters. Conversely, local Nusselt number is suppressed with increment in Brownian motion and thermophoresis parameters (N_b and N_t) since these nanoscale effects assist to heat boundary-layer and reduce thermal transport to wall. Heat transfer rates can therefore be controlled very effectively by judicious selection of these thermophysical parameters. **Table 4** displays the aspects of distinct mass diffusion variables on Sherwood number $Sh_x\,\mathrm{Re}_x^{-\frac{1}{2}}$. It is apparent that $Sh_x\,\mathrm{Re}_x^{-\frac{1}{2}}$ is enhanced with elevation in Sc, S_2, N_b and γ_2 i.e. greater values of Sc, S_2 and N_b. Conversely a strong decrement in local Sherwood number $Sh_x\,\mathrm{Re}_x^{-\frac{1}{2}}$ is induced by increasing thermophoresis parameter N_t indicating a depletion in nano-particle mass diffusion to wall, associated with greater concentration boundary-layer thickness and greater concentration magnitudes in the boundary-layer induced through stronger thermophoretic body force effect. reduced the value of the Sherwood numbers. Finally, the

comparative outcomes authenticating reliability of utilized technique are reported through **Table 5.** Here the obtained (HAM) outcomes are found in good agreement.

6. CONCLUSIONS

A mathematical study has been elaborated for the influence of convected thermosolutal boundary conditions and dual thermo/solutal (double) stratification on the dual convective flow of tangent hyperbolic nanoliquid from a permeable stretched surface subject to heat generation/absorption and radiative flux, as a simulation of high temperature nano-polymeric materials processing. The hyperbolic tangent non-Newtonian two-parameter model has been employed along with Rosseland diffusion flux model deployed for radiative heat-transfer. Buongirono's two-component nanoscale model has been utilized for nanofluid behaviour. The principal outcomes of current simulations are:

(i) Temperatures and thermal boundary-layer thicknesses are increased with augmentation in radiative, thermophoresis, Brownian motion, thermal Biot number and heat generation parameters whereas they are reduced with increasing thermal stratification parameter.

(ii) Nano-particle concentration values and concentration boundary-layer thicknesses are suppressed with greater Schmidt number, Brownian movement and solutal stratification variable whereas they are improved with greater estimations of thermophoretic and concentration Biot number.

(iii) A rise in material parameter and wall suction the flow is slowed (momentum boundary-layer thickness is reduced) whereas flow is accelerated (momentum boundary-layer thickness diminished) with growing nonlinear thermal convective parameter, wall injection, mixed convection parameter and buoyancy ratio values.

(iv) Local Nusselt number is strongly increased with greater Prandtl number, thermal stratification number, thermal Biot number and radiative parameter.

(v) Coefficient of skin-friction is suppressed with a rise in tangent hyperbolic rheological power-law index, material and buoyancy parameters.

(vi) Shear stress and heat-mass transport rates at permeable sheet (wall) can be effectively manipulated by nano-polymer rheological characteristics, buoyancy force interplay, nanoscale and thermo/solutal stratification mechanisms, which can be exploited in materials processing operations.

The study has demonstrated the excellent efficiency of HAM in nonlinear thermal nano-polymeric coating flow dynamic simulation. However, attention has been limited to a simple radiative flux model (Rosseland). The results of viscous nanoliquid model can be acquired in the absence of material variable and power-law index. Future studies may examine more elegant radiative transfer models e. g. Chandrasekhar discrete ordinates model (DOM), two-flux models etc, and will be communicated imminently.

Declaration of Competing Interest

The authors declare that they have no known competing financial interests or personal relationships that could have appeared to influence the work reported in this paper.

Acknowledgement

The authors would like to thank the Deanship of Scientific Research at Umm Al-Qura University for supporting this work via **Grant Code:22UQU4331317DSR**.

REFERENCES

[1] Bartosik, A., Application of rheological models in prediction of turbulent slurry flow, *Flow, Turbulence and Combustion*, 277-293, 84 (2010).

[2] Shenoy, A.V. (1999). *Rheology of Filled Polymer Systems*, Springer, USA.

[3] E. Brujan, *Cavitation in Non-Newtonian Fluids with Biomedical and Bioengineering Applications,* Springer, Germany (2011).

[4] De Blasio F.V. Non-Newtonian fluids, mudflows, and debris flows: a rheological approach. *In: Introduction to the Physics of Landslides.* Springer, Dordrecht (2011).

[5] W.R. Schowalter, *Mechanics of Non-Newtonian Fluids*, Pergamon Press, Oxford (1978).

[6] R.B. Bird, R.C. Armstrong and O. Hassager, *Dynamics of Polymeric Liquids, Volume 1: Fluid Mechanics*, 672 Pages, Wiley, USA (1987).

[7] Y. Jaluria, Heat and mass transfer in materials processing and manufacturing, *Advances in Heat Transfer*, 48, 1-94 (2016).

[8] Mahanthesh, B., Kumar, P. S., Gireesha, B. J., Manjunatha, S., & Gorla, R. S. R. (2017). Nonlinear convective and radiated flow of tangent hyperbolic liquid due to stretched surface with convective condition. Results in Physics, 7, 2404-2410.

[9] Kumaran, G., Sivaraj, R., Prasad, V.R., **O. Anwar Bég**, Leung, H.H., and Kamalov, F. (2021). Numerical study of axisymmetric magneto-gyrotactic bioconvection in non-Fourier tangent hyperbolic nano-functional reactive coating flow of a cylindrical body in porous media. The European Physical Journal Plus, 136, 1107.

[10] Hussain, S.M., and Jamshed, W. (2021). A comparative entropy based analysis of tangent hyperbolic hybrid nanofluid flow: Implementing finite difference method. International Communications in Heat and Mass Transfer, 129, 105671.

[11] Prakash, J., Tripathi, D., Akkurt, N., and **O. Anwar Bég** (2022). Tangent hyperbolic non-Newtonian radiative bioconvection nanofluid flow from a bi-directional stretching surface with electro-magneto-hydrodynamic, Joule heating and modified diffusion effects. The European Physical Journal Plus, 137, 472.

[12] Choi S.U.S., Enhancing thermal conductivity of fluids with nanoparticles *Developments Applications of Non-Newtonian Flows FED-vol 231/MD-vol 66* ed D A Siginer and H P Wang (New York: ASME) pp 99-105 (1995).

[13] Das S K, Choi S U S and Patel H. E., Heat transfer in nanofluids-a review, *Heat Transfer Eng.* 27, 2-19 (2006).

[14] Afeez O.Gbadamosi *et al.*, Recent advances and prospects in polymeric nanofluids application for enhanced oil recovery, *J. Industrial and Engineering Chemistry*, 66, 1-19 (2018).

[15] K.S.Pavithra *et al*., Polymer-dispersant-stabilized Ag nanofluids for heat transfer applications, *J. Thermal Analysis and Calorimetry*, 146, 601–610 (2021).

[16] J. Buongiorno, Convective transport in nanofluids, *ASME J. Heat Transfer*, 128 (3) 240-250 (2006).

[17] H. Chen *et al*., Rheological behaviour of nanofluids, *New J. Phys.* 9, 367 (2007).

[18] Tseng W J and Lin K C., Rheology and colloidal structure of aqueous TiO_2 nanoparticle suspensions *Mater. Sci. Eng.* A 355 186-92 (2003).

[19] Yang Y, Grulke E A, Zhang Z G and Wu G F., Thermal and rheological properties of carbon nanoturbe-in-oil dispersions *J. Appl. Phys.* 99 114307 (2006).

[20] Atif, S. M., Hussain, S., & Sagheer, M. (2019). Heat and mass transfer analysis of time-dependent tangent hyperbolic nanofluid flow past a wedge. *Physics Letters A*, *383*(11), 1187-1198.

[21] Salahuddin, T., Malik, M. Y., Hussain, A., Awais, M., Khan, I., & Khan, M. (2017). Analysis of tangent hyperbolic nanofluid impinging on a stretching cylinder near the stagnation point. *Results in physics*, *7*, 426-434.

[22] Shahzad, F., Sagheer, M., & Hussain, S. (2019). MHD tangent hyperbolic nanofluid with chemical reaction, viscous dissipation and Joule heating effects. *AIP Advances*, *9*(2), 025007.

[23] Shafiq, A., Hammouch, Z., & Sindhu, T. N. (2017). Bioconvective MHD flow of tangent hyperbolic nanofluid with Newtonian heating. *International Journal of Mechanical Sciences*, *133*, 759-766.

[24] H. Thameem Basha, R. Sivaraj, V. R. Prasad, **O. Anwar Bég**, Entropy generation of tangent hyperbolic nanofluid flow over a circular cylinder in the presence of nonlinear Boussinesq approximation: A non-similar solution, *J. Thermal Analysis and Calorimetry (2020).* https://doi.org/10.1007/s10973-020-09981-5

[25] G. Kumaran, R Sivaraj, V. Ramachandra Prasad, **O. Anwar Bég**, Numerical study of axisymmetric magneto-gyrotactic bioconvection in non-Fourier tangent hyperbolic nano-functional reactive coating flow of a cylindrical body in porous media, *European Physical Journal Plus*, 136, 1107 (2021). https://doi.org/10.1140/epjp/s13360-021-02099-z (32 pages)

[26] Awais, M., Kumam, P., Ali, A., Shah, Z., & Alrabaiah, H. (2020). Impact of activation energy on hyperbolic tangent nanofluid with mixed convection rheology and entropy optimization. *Alexandria Engineering Journal*. https://doi.org/10.1016/j.aej.2020.10.036.

[27] Makinde, O.D., Mabood, F. and Ibrahim, M.S. (2018). Chemically reacting on MHD boundary layer flow of nanofluid over a non-linear stretching sheet with heat source/sink and thermal radiation. Thermal Science, 22, 495-506.

[28] Eid, M. R. and Makinde, O. D. (2018). Solar radiation effect on a magneto nanofluid flow in a porous medium with chemically reactive species. International Journal of Chemical Reactor Engineering, 16, https://doi.org/10.1515/ijcre-2017-0212.

[29] Mahanthesh, B., Gireesha, B.J., Gorla, R.S.R. and Makinde, O. D. (2018). Magnetohydrodynamic three-dimensional flow of nanofluids with slip and thermal radiation over

a nonlinear stretching sheet: a numerical study. Neural Computing and Applications, 30, 1557-1567.

[30] Narayana, P.V.S., Tarakaramu, N., Makinde, O.D., Venkateswarlu, B. and Sarojamma, G. (2018). MHD stagnation point flow of viscoelastic nanofluid past a convectively heated stretching surface. Defect and Diffusion Forum, 387, 106-120.

[31] Jayavel, P., Tripathi, D., **Beg, O. Anwar**, Tiwari, A.K. and Kumar, R. (2021). Thermo-electrokinetic rotating non-Newtonian hybrid nanofluid flow from an accelerating vertical surface. *Heat Transfer,* https://doi.org/10.1002/htj.22373 .

[32] Saleem, N., Munawar, S. and Tripathi, D. (2021). Entropy analysis in ciliary transport of radiated hybrid nanofluid in presence of electromagnetohydrodynamics and activation energy. Case Studies in Thermal Engineering, 28, 101665.

[33] W. Ibrahim and O.D. Makinde, The effect of double stratification on boundary-layer flow and heat transfer of nanofluid over a vertical plate, *Computers & Fluids*, 86, 433-441 (2013).

[34] Farooq, M., Javed, M., Khan, M. I., Anjum, A., & Hayat, T. (2017). Melting heat transfer and double stratification in stagnation flow of viscous nanofluid. *Results in physics*, *7*, 2296-2301.

[35] Rehman, K. U., Malik, A. A., Malik, M. Y., Sandeep, N., & Saba, N. U. (2017). Numerical study of double stratification in Casson fluid flow in the presence of mixed convection and chemical reaction. *Results in Physics*, *7*, 2997-3006.

[36] Ahmad, S., Farooq, M., Javed, M., & Anjum, A. (2018). Double stratification effects in chemically reactive squeezed Sutterby fluid flow with thermal radiation and mixed convection. *Results in physics*, *8*, 1250-1259.

[37] Shah, N. A., Ahmed, N., Vieru, D., & Fetecau, C. (2019). Effects of double stratification and heat flux damping on convective flows over a vertical cylinder. *Chinese Journal of Physics*, *60*, 290-306.

[38] Ijaz, M., & Ayub, M. (2019). Activation energy and dual stratification effects for Walter-B fluid flow in view of Cattaneo-Christov double diffusionon. *Heliyon*, *5*(6), e01815. https://doi.org/10.1016/j.heliyon.2019.e01815

[39] Mallawi, F. O. M., Bhuvaneswari, M., Sivasankaran, S., & Eswaramoorthi, S. (2020). Impact of double-stratification on convective flow of a non-Newtonian liquid in a Riga plate with Cattaneo-Christov double-flux and thermal radiation. *Ain Shams Engineering Journal*. https://doi.org/10.1016/j.asej.2020.04.010

[40] Tlili, I., Ramzan, M., Nisa, H. U., Shutaywi, M., Shah, Z., & Kumam, P. (2020). Onset of gyrotactic microorganisms in MHD Micropolar nanofluid flow with partial slip and double stratification. *Journal of King Saud University-Science*, *32*(6), 2741-2751.

[41] Ali, U., Malik, M. Y., Alderremy, A. A., Aly, S., & Rehman, K. U. (2020). A generalized findings on thermal radiation and heat generation/absorption in nanofluid flow regime. *Physica A: Statistical Mechanics and its Applications*, 124026. https://doi.org/10.1016/j.physa.2019.124026

[42] Goud, B. S. (2020). Heat generation/absorption influence on steady stretched permeable surface on MHD flow of a micropolar fluid through a porous medium in the presence of variable suction/injection. *International Journal of Thermofluids*, *7*, 100044. https://doi.org/10.1016/j.ijft.2020.100044

[43] **O. Anwar Bég**, W.A. Khan and M.J. Uddin, Multiple slip effects on unsteady magnetohydrodynamic nanofluid transport with heat generation/absorption effects in temperature dependent porous media, *J. Porous Media,* 18, 907-922 (2015).

[44] Irfan, M., & Farooq, M. A. (2020). Thermophoretic MHD free stream flow with variable internal heat generation/absorption and variable liquid characteristics in a permeable medium over a radiative exponentially stretching sheet. *Journal of Materials Research and Technology*. https://doi.org/10.1016/j.jmrt.2020.03.005

[45] **O. Anwar Bég**, K. Venkatadri, V.R. Prasad, T. A. Bég, A. Kadir and **Henry J. Leonard**, Numerical simulation of hydromagnetic Marangoni convection flow in a Darcian porous semiconductor melt enclosure with buoyancy and heat generation effects, *Materials Science and Engineering B: Advanced Functional and Solid-State Materials*, 261, (2020) 114722. (23 pages)

[46] Kou S., *Transport Phenomena in Materials Processing*, Wiley, New York, USA(1996).

[47] Hayat, T., Khan, M. I., Waqas, M., & Alsaedi, A. (2017). On the performance of heat absorption/generation and thermal stratification in mixed convective flow of an Oldroyd-B fluid. *Nuclear Engineering and Technology*, *49*(8), 1645-1653.

[48] Ramesh, K., Tripathi, D., Bhatti, M.M. and Khalique, C.M. (2020). Electro-osmotic flow of hydromagnetic dusty viscoelastic fluids in a microchannel propagated by peristalsis, Journal of Molecular Liquids, 314, 113568.

[49] Manzur, M., ur Rahman, M., & Khan, M. (2020). Computational study of Falkner–Skan flow of chemically reactive Cross nanofluid with heat generation/absorption. *Physica A: Statistical Mechanics and its Applications*, 124267. https://doi.org/10.1016/j.physa.2020.124267

[50] Balaji, R., Prakash, J., Tripathi, D. and **O. Anwar Bég** (2022). Computation of magnetohydrodynamic electro-osmotic modulated rotating squeezing flow with zeta potential effects, *Colloids and Surfaces A: Physicochemical and Engineering Aspects* 640, 128430.

[51] Bhandari, D.S., Tripathi, D. and Prakash, J. (2022). Insight into Newtonian fluid flow and heat transfer in vertical microchannel subject to rhythmic membrane contraction due to pressure gradient and buoyancy forces, International Journal of Heat and Mass Transfer 184, 122249.

[52] Liao, S. (2010). An optimal homotopy-analysis approach for strongly nonlinear differential equations. *Communications in Nonlinear Science and Numerical Simulation*, *15*(8), 2003-2016.

[53] Rehman, K. U., Alshomrani, A. S., Malik, M. Y., Zehra, I., & Naseer, M. (2018). Thermo-physical aspects in tangent hyperbolic fluid flow regime: a short communication. Case studies in thermal engineering, 12, 203-212.

[54] S. Satish, Nano polymer films by fast dip coating method for field effect transistor applications, *Physics Procedia*, 49, 166-176 (2013).

[55] M.F. Modest, *Radiation Heat Transfer*, MacGraw-Hill, New York, USA (1993).

[56] D. Tripathi and **O. Anwar Bég**, Peristaltic transport of Maxwell viscoelastic fluids with a slip condition: Homotopy analysis of gastric transport, *J. Mechanics Medicine Biology, 15 (3)* 1550021.1- 1550021.22 (2015).

[57] A. K. Ray, B Vasu, **O. Anwar Bég**, R. S R Gorla and P. V. S. N. Murthy, Homotopy semi-numerical modelling of non-Newtonian nanofluid transport external to multiple geometries using a revised Buongiorno model, *Inventions, 4, 54, 1-27 (2019). doi:10.3390/inventions4040054*

[58] Ibrahim, S.M., Kumar, P.V. and Makinde, O.D. (2019). Chemical reaction and radiation effects on non-Newtonian fluid flow over a stretching sheet with non-uniform thickness and heat source, Defect and Diffusion Forum, 387, 319-331.